



Article

Mechanical Properties of Strengthening 5083-H111 Aluminum Alloy Plates at Elevated Temperatures

Wael Abuzaid ¹, Rami Hawileh ^{2,*}  and Jamal Abdalla ²

¹ Department of Mechanical Engineering, American University of Sharjah, P.O. Box 26666 Sharjah, United Arab Emirates; wabuzaid@aus.edu

² Department of Civil Engineering, American University of Sharjah, P.O. Box 26666 Sharjah, United Arab Emirates; jabdalla@aus.edu

* Correspondence: rhaweeleh@aus.edu

Abstract: The use of aluminum alloys for external strengthening of reinforced concrete (RC) beams has been capturing research interest. Exposure to harsh environmental conditions can severely impact the strengthening efficiency. This work aims to investigate the degradation in the mechanical properties of aluminum alloy AA 5083 plates when exposed to temperatures ranging from 25 to 300 °C. Quasi-static Isothermal tensile experiments were conducted at different temperatures. It was observed from the experimental results that the yield strength remained constant in the temperature range of 25–150 °C before starting to drop beyond 150 °C, with a total reduction of ≈40% at 300 °C. The elastic modulus was temperature sensitive with about 25% reduction at 200 °C before experiencing a significant and pronounced reduction at 300 °C. The percentage drops in stiffness and yield strength at 300 °C were 62.8% and 38%, respectively. In addition, the Mechanical Threshold Strength Model (MTS) parameters were established to capture the yield strength temperature dependence. Two analytical models were developed based on the experimental results. Both models can reasonably predict the elastic modulus and yield strength of AA 5083 plates as a function of temperature. It was concluded that AA plates should be properly insulated when used as externally bonded reinforcement to strengthen RC beams.

Keywords: aluminum alloy; strengthening; elevated temperatures; digital image correlation; elastic modulus; yield strength; mechanical threshold strength



Citation: Abuzaid, W.; Hawileh, R.; Abdalla, J. Mechanical Properties of Strengthening 5083-H111 Aluminum Alloy Plates at Elevated Temperatures. *Infrastructures* **2021**, *6*, 87. <https://doi.org/10.3390/infrastructures6060087>

Academic Editor: Chris Goodier

Received: 26 May 2021
Accepted: 11 June 2021
Published: 14 June 2021

Publisher's Note: MDPI stays neutral with regard to jurisdictional claims in published maps and institutional affiliations.



Copyright: © 2021 by the authors. Licensee MDPI, Basel, Switzerland. This article is an open access article distributed under the terms and conditions of the Creative Commons Attribution (CC BY) license (<https://creativecommons.org/licenses/by/4.0/>).

1. Introduction

In regions with humid environments, many reinforced concrete (RC) structures suffer from deterioration. This is due to a phenomenon called rust expansion which accelerates the rate of corrosion of steel reinforcement and simulates the cracking and peeling of the protective concrete cover; eventually, leading to structural failure [1]. One approach to recover and retrofit buildings and structures exposed to humid/coastal environments is to use natural fibers as a reinforcement element in mortars. This approach proved to reduce concrete cracks and increase the ductility and stiffness of the treated structural members. However, due to variations between the composites and mortars, there is an issue of interfacial adhesion between the reinforcement and cementitious matrix [2]. Another viable solution to enhance the structural performance of deteriorated structures is to externally strengthen the RC members with metal or composites plates/sheets. Some metals and composites are used in external strengthening applications such as steel, aluminum, and composite fiber reinforced polymer (FRP) laminates.

Aluminum alloys (AA) are increasingly being considered in various applications due to their desirable mechanical properties, lightweight, and good corrosion resistance [3–6]. Despite the wide adoption in many industries, the interest in using aluminum all-oyes (AA) as external strengthening materials for RC structures is recent [7,8]. Traditionally, steel plates have been used to externally strengthen RC structures. However, its heavy

weight and poor corrosion resistance properties have made it an unviable material in strengthening applications. More recently, fiber reinforced polymers (FRP) were applied as externally bonded reinforcement to strengthen RC members. Despite its numerous advantages, such as high strength to weight ratios and corrosion resistance, FRP materials lack ductility [9,10]. The utilization of aluminum alloys as externally bonded strengthening material can address these limitations. However, the degradation of properties at elevated temperatures poses a fire resistance concern. When structural members are exposed to high temperature levels, the overall stiffness significantly reduces as a result of degradation in the mechanical properties of the materials, which results in overall structural failure [11]. Under such conditions, full assessment of mechanical properties, particularly yield strength and stiffness, are advantageous for design engineers to help minimize the risk associated with accidents involving fire and high temperatures. This work addresses these issues by conducting an experimental study dedicated to quantify the degradation in mechanical properties of AA 5083 at elevated temperatures. In addition, analytical models providing predictive capability of the temperature dependent yield strength and elastic modulus are evaluated.

AA5083-H111 marine-grade aluminum alloy is primarily used in the fabrication of ships, water vehicles, and vessels. In recent works, researchers have experimentally and numerically explored the use of this alloy in external strengthening of RC beams in shear [12–15] and in flexure [16–18]. Recently, AA bars have been used successfully as a Near Surface Mounted (NSM) flexural strengthening material for reinforced concrete beams [19–21]. The utilized AA plates and bars have similar yield strength, tensile strength, and ductility to that of steel plates, and comparable high corrosion resistance to that of FRP laminates. Test results have shown a significant enhancement in the strength of strengthened RC beam specimens, up to 40% in flexure and 89% in shear. In addition, the beams' ductility significantly surpassed that of carbon fiber reinforced polymers (CFRP) laminates. Most of the aforementioned experimental investigations were conducted at room temperature. The performance of AA5083 plates as a strengthening material exposed to elevated temperature has not been investigated. However, before implementing this material in the construction and strengthening market, the relevant mechanical properties of AA5083 plates such as tensile strength, modulus of elasticity, and elongation need to be investigated at elevated temperatures. This paper examines these mechanical properties of AA5083 plates at temperature ranging between 25 and 300 °C.

Various aspects of the high-temperature performance of this alloy have been investigated in previous studies [22–29]. Summers et al. [22,23] studied post-fire residual mechanical properties of 5083-H116, 6082-T651, and 6082-T6 aluminum alloy extrusions. After exposing the alloys to elevated temperatures, tension tests and Vickers hardness measurements tests were performed to determine the mechanical response of the alloys and quantify the time and temperature-dependent behavior. Chen et al. [24] investigated the hot deformation resistance of an AA5083 alloy under high strain rate. They made quantitative analyses over the effects of temperature, strain rate, and work hardening behavior on the flow curves and developed a modified constitutive equation for prediction of hot deformation resistance of the AA5083 alloy at high temperatures and high strain rate. Summers et al. [25] developed a comprehensive model to predict the residual constitutive behavior of AA5083-H116 at room temperature following fire exposure. The predictions of the residual yield strength and strain hardening of the developed constitutive model showed good agreement with that of the experimental results. Free et al. [26] carried an experimental investigation to study the change in microstructure and mechanical properties of six different 5000 series aluminum alloys following a simulated fire exposure. Guo et al. [27] studied the mechanical properties of certain brands of aluminum alloys (AA6061, AA6082, AA6N01, AA7020) at temperatures that ranged from –100 to 300 °C. They concluded that the AA strength and ductility improved at low temperatures and their mechanical properties (elastic modulus, ultimate strength, nominal yield strength) dropped rapidly at high temperatures. In addition, they observed clear changes in the deformation

mechanisms of AA at extreme temperatures [27]. Huda et al. [28] investigated the hardness behavior of aluminum alloy 2024-T3 through microstructural characterization and heat treatment experiments (temperature effects) involving annealing in the temperature range of 100–250 °C for a time duration of 2–22 h. They concluded that the 2024-T3 aluminum alloy revealed a multiphase microstructure and showed no softening at short time of annealing (10 h) and low temperatures (100 °C). On the other hand, they observed that it showed softening with longer time-durations of exposures to the temperature and initial hardening followed by rapid softening at higher temperature (200 °C). At the highest annealing temperature (250 °C), the material first softened rapidly, and then the rate of softening decreased with the increase in time of exposures to temperature [28]. Prakash et al. [29] carried out an experimental investigation on the deformation behaviors of the aluminum alloy Al5052-H32 under tensile, compressive, and flexure loads at different strain rates and different temperatures (25, 250, 350, and 450 °C). They concluded that under quasi-static tensile loads, the flow stress of the alloy decreases but its ductility increases with increasing temperature. In addition to that, it was observed that the alloy has mixed brittle–ductile fracture at high temperatures (350 and 450 °C) [29]. Although there are other investigators who embarked on studying the behavior of aluminum alloys at elevated temperatures; however, to the authors' knowledge, the literature is lacking full experimental assessment of the mechanical properties of AA5083 at elevated temperatures along with predictive models capable of capturing the temperature degrading effects on the elastic modulus and the yield strength. This limitation will hinder the wide-spread use and application of AA 5083 plates as external strengthening materials in the construction market, especially when the effect of temperature has to be taken into consideration.

To predict the degrading temperature effects on the yield strength, a constitutive model that is valid at various temperatures is needed. The physically-based Mechanical Threshold Strength Model (MTS) provides the capability to capture the constitutive response over a wide range of temperatures and strain rates [30,31]. Successful utilization, with good predictive capability, of the MTS model has been reported for various metallic alloys such as AISI 4340 steel [32], AA 5182 [33], AA 6061 [34], and AA5083 [35] aluminum alloys. Ma et al. [35] investigated the influence of fire exposure on mechanical properties of AA5083 using experimental and finite element simulations. They utilized the MTS model for defining the properties of AA5083 before and after exposure to fire. However, the model parameters have not been well established for the AA 5083-H111 alloy. The model can be calibrated using stress–strain data collected at different temperatures and strain rates. The final outcome is a rather simple equation that can predict the flow stress as a function of temperature, strain rate, and deformation history. In this work, the aim is to get a good estimate of the temperature effects on the flow stress at a constant, quasi-static strain rate, and no plastic strain history. This will yield the temperature dependent yield strength which describes initial yielding at different loading temperatures. Providing predictive capability, through physics-based modeling, is advantageous for design engineers considering this alloy for strengthening applications.

In summary, this work aims to investigate experimentally and analytically the degradation in mechanical properties of AA plates, type 5083-H111, when subjected to temperatures ranging from 25 to 300 °C. The experimental results and the calibrated predictive models are of practical importance and can assist in the analysis and design of RC members externally strengthened with such aluminum alloy plates in shear and flexure when subjected to elevated temperatures.

2. Materials and Methods

AA 5083-H111 aluminum sheets (3 mm thickness) were used in this study. The initial microstructure of the rolled alloy was characterized using electron backscatter diffraction (EBSD) as shown in Figure 1a. A region of $\approx 3000 \times 2300 \mu\text{m}^2$ was scanned using a step size of 2 μm . The grain orientation map and pole figures of the scanned area are shown

in Figure 1b,c. The average grain size (diameter) of the material was $\approx 33 \mu\text{m}$ as extracted from the grain size distribution shown in Figure 1d.

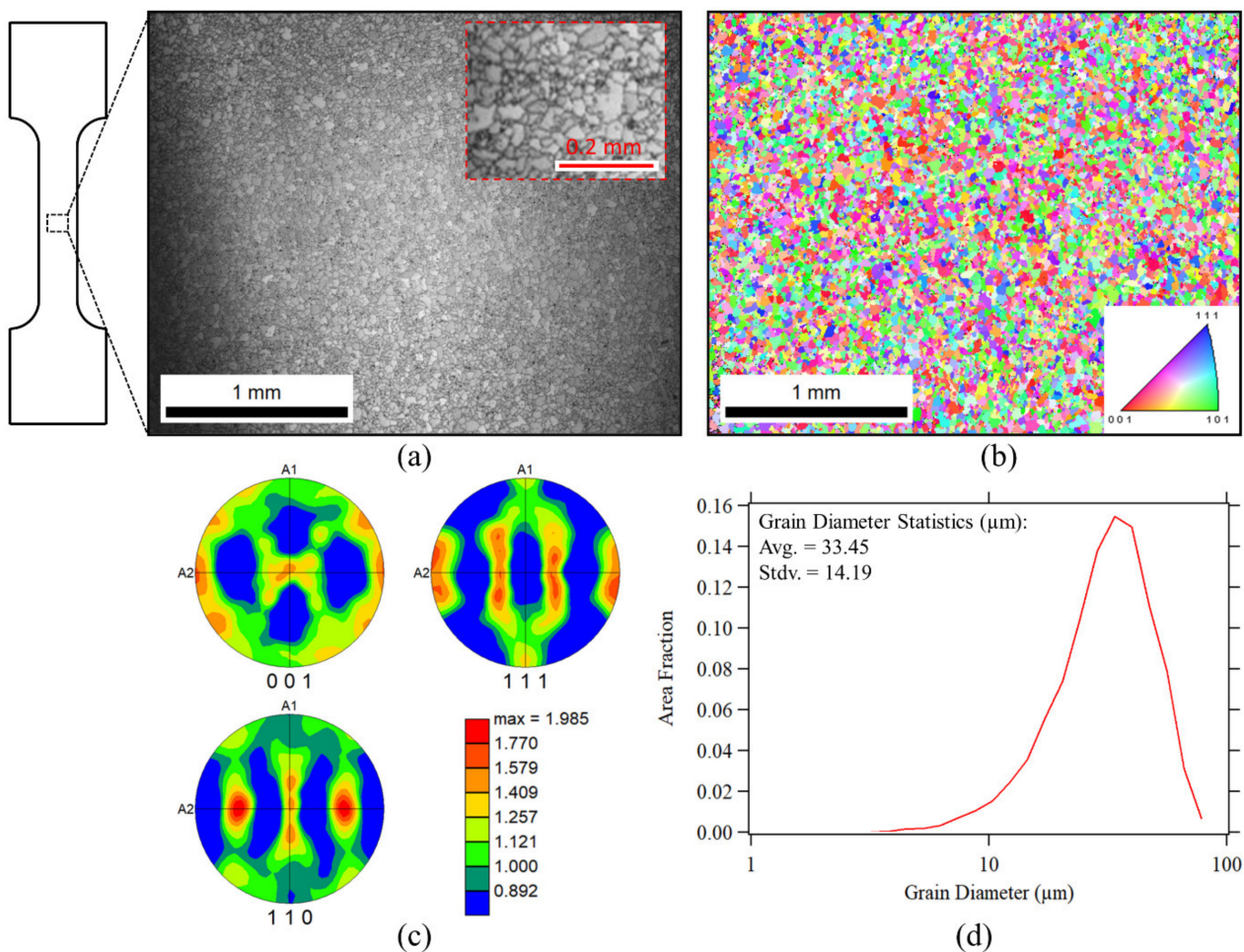


Figure 1. Characterization of AA 5083-H111 aluminum sheets. (a) SEM micrograph showing the initial microstructure of the AA 5083-H111 rolled aluminum sheet; (b) Grain orientation map of the region shown in (a); (c) Pole figure; (d) Histogram showing the grain size distribution in the scanned area.

Dogbone tension samples with $8 \times 3 \text{ mm}^2$ gauge section, schematically shown in Figure 2a, were machined from the as-received sheets. To allow for full-field strain measurements using digital image correlation (DIC), the surface of each sample was polished using SiC grinding paper (up to 1000 grit) to remove any surface scratches. The speckle pattern for DIC was subsequently applied to the surface using high-temperature black paint. The quality and stability of the DIC pattern were suitable for the temperatures considered in this work (up to $300 \text{ }^\circ\text{C}$) with no noticeable pattern degradation during the span of each experiment. DIC reference and deformed images were captured using a high-resolution optical camera with an imaging resolution of $\approx 140 \text{ pixels/mm}$.

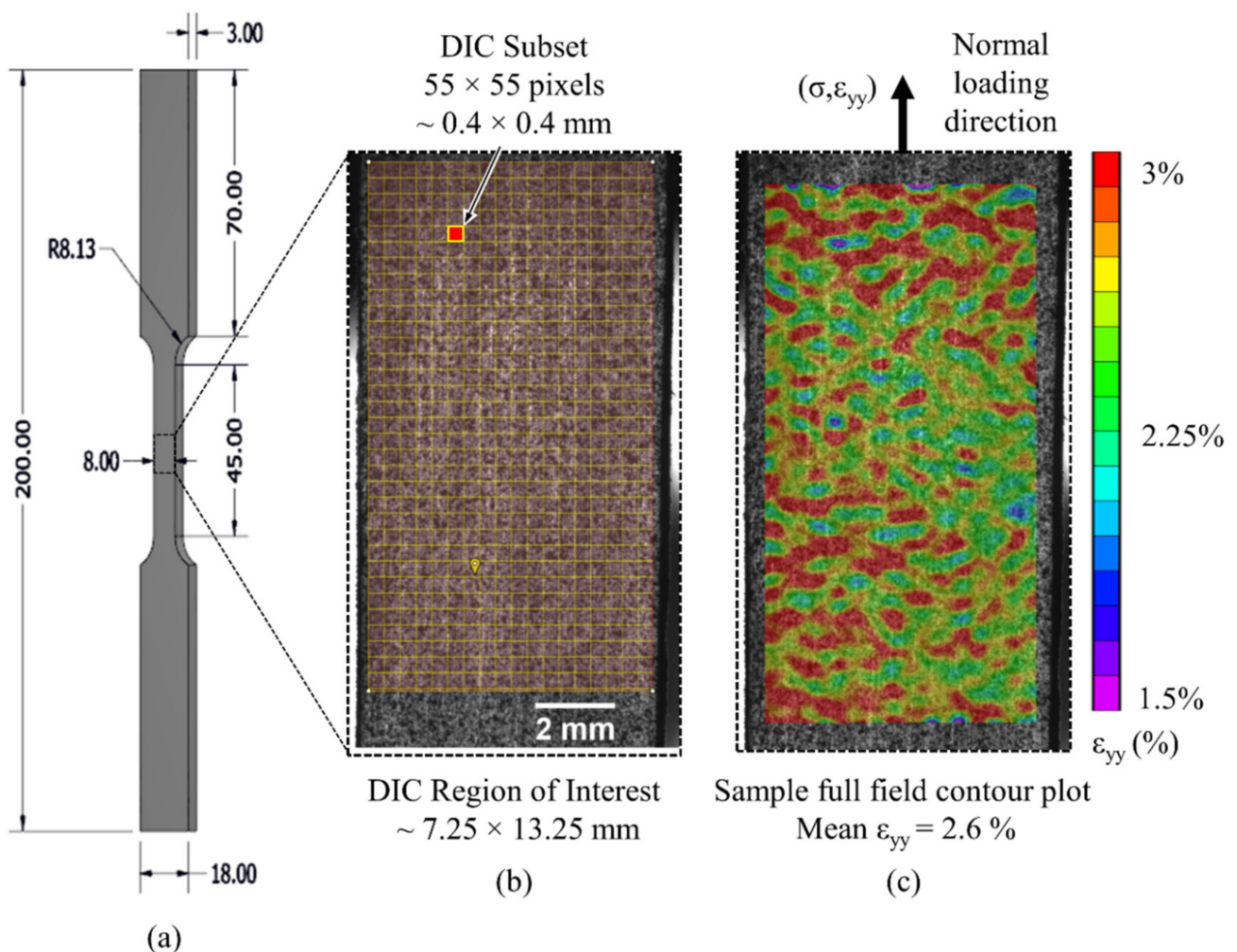


Figure 2. (a) Dogbone tensile sample schematic; (b) A representative region of interest for DIC correlations; (c) Full field contour plot of the normal strain field along the loading direction taken at 2.6% during loading (all dimensions are in mm).

Isothermal tension experiments were conducted using an Instron servo-hydraulic load frame equipped with an environmental chamber (i.e., heating furnace). Samples were installed in load control (set to zero load after gripping the sample) to prevent deformation during heating inside the oven (i.e., due to thermal expansion). Once the desired temperature was reached, and to assure uniform temperature distribution, 45 min heating time elapsed before mechanical loading was started. Tensile loading was conducted in displacement control at a rate of 1 mm/min which corresponds to an average strain rate of $3 \times 10^{-4} \text{ s}^{-1}$ (established subsequently from DIC mean strains along the loading direction). During loading, deformed images were captured every 2 s. A data acquisition system was used to collect and save the applied force and displacement data at the moment each of the optical images were captured. All samples were loaded to fracture, however, DIC data were collected for about 6% strain which was sufficient to extract the parameters of interest in this work (elastic modulus and yield strength).

All correlations were based on a region of interest (ROI) of $\approx 7.25 \times 13.25 \text{ mm}$ with a DIC subset size of 55 pixels ($\approx 0.4 \text{ mm}$) and 5-pixel subset spacing. A representative ROI is shown in Figure 2b with the corresponding subset size used in this work. Full field contour plots of the normal ϵ_{yy} , ϵ_{xx} , and ϵ_{xy} strains can be generated from each of the deformed images. A sample contour plot for the normal strain field is shown in Figure 2c. The mean strain can be calculated for each image/contour plot. Calculating the mean strain along the loading direction, mean ϵ_{yy} , is analogous to what can be obtained using an extensometer.

All the DIC strains reported in this work represent field averages obtained from the ϵ_{yy} full field data.

3. Results and Analysis

3.1. Isothermal Tension Experiments

Isothermal tension experiments were conducted at room temperature (RT \approx 25 °C), 75, 100, 150, 200, 250, and 300 °C. Figure 3 shows representative stress–strain curves for selected samples (others omitted from the figure for clarity). The reported strains were obtained from full-field mean averages as explained previously. An obvious degradation in the modulus and yield strength can be observed from the reported results, particularly at 300 °C. As noted previously, loading was conducted to failure although DIC strain data were only collected up to about 6%. To construct the full stress–strain curve, a correlation is established between the measured strains, using DIC, and the reported load frame displacements for every prescribed temperature.

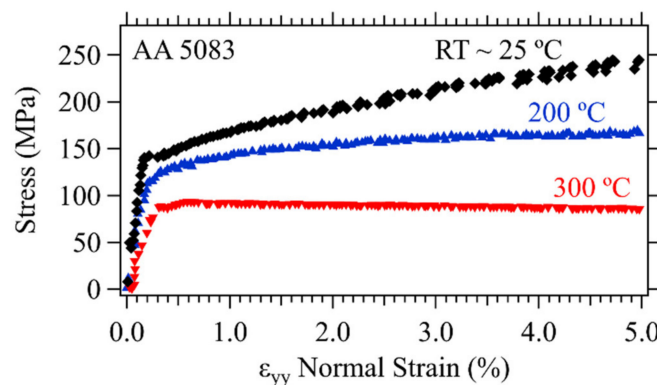


Figure 3. Stress–strain curves at different temperature conditions, representative cases. The reported strains were obtained from DIC full field averages as shown in Figure 2c.

Figure 4 shows a sample plot of DIC strains versus load frame displacement. A linear fit to the results yields a factor that can be multiplied by the machine displacement to estimate the corresponding normal strain ϵ_{yy} . For the data reported in Figure 4, a factor of 1.6927 was calculated. A similar analysis was conducted for each of the samples reported in this work. Stress–strain curves generated using this technique are reported in Figure 5 for selected temperature conditions. A typical increase in ductility and reduction in the hardening rate, and even softening at 300 °C, is observed with temperature increase.

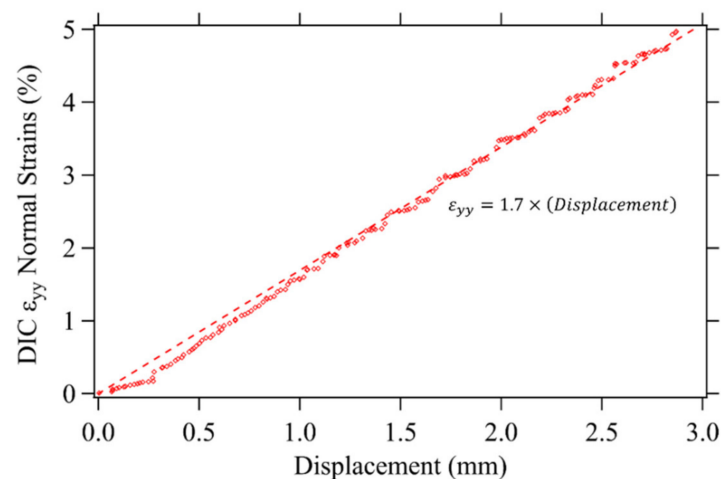


Figure 4. DIC mean ϵ_{yy} strain versus load frame displacement. A linear fit establishes the conversion relation between these parameters.

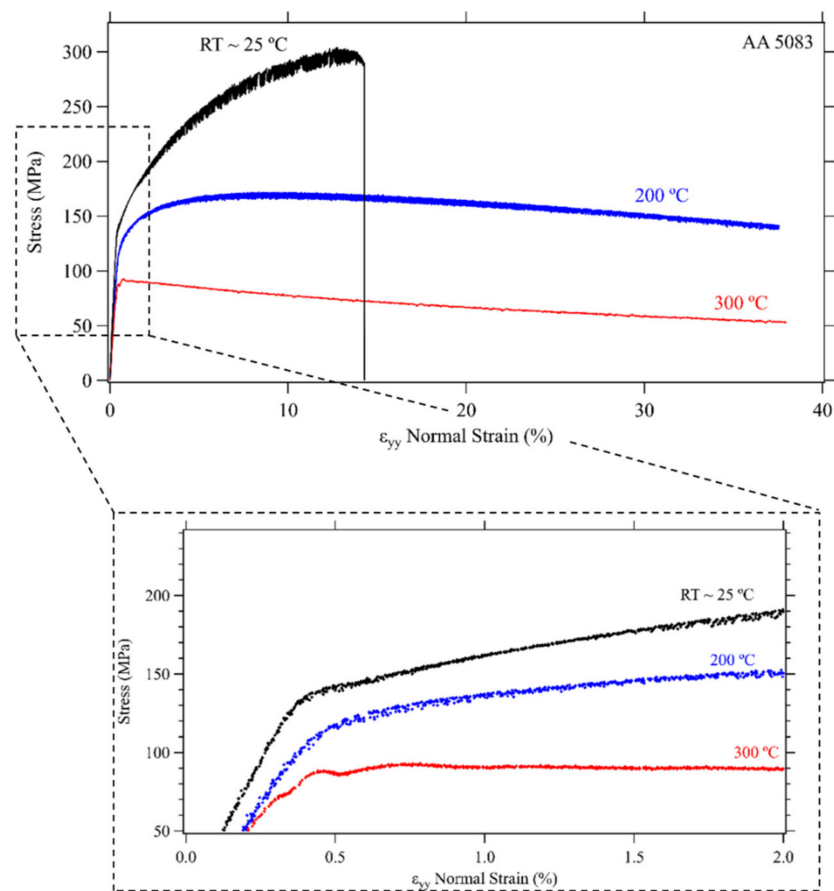


Figure 5. Stress–strain curves at different temperature conditions, representative cases. The reported strains were obtained from the load frame displacements and the conversion relations established in Figure 4 for one of the cases.

This work is primarily concerned with the elastic modulus and yield strength changes as a function of temperature. Those parameters are required in the analysis and design of reinforced concrete beams and slabs externally strengthened with such AA plates. These magnitudes were extracted from the stress–strain curves (DIC strains) using the slope of the elastic region for the elastic modulus E and the standard 0.2% offset for the yield strength σ_y , as shown in Figure 6. These magnitudes are reported for the 75 °C case in Figure 6 and for the rest of the temperature conditions in Table 1.

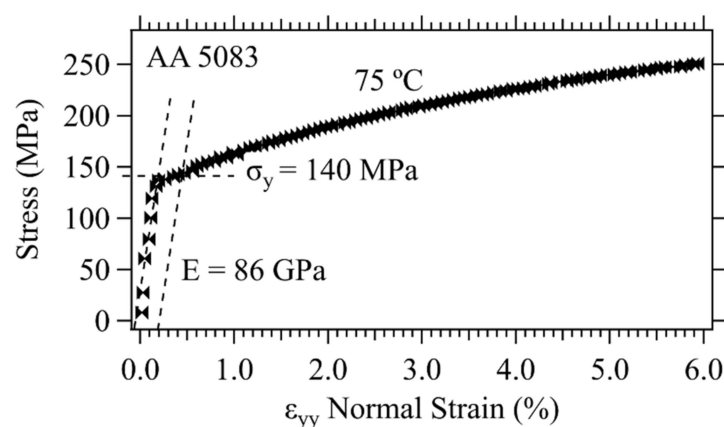


Figure 6. Stress–strain curves 75 °C. The elastic modulus, E , was calculated using the slope of the elastic region and the yield strengths using the 0.2% offset.

Table 1. Yield strength and elastic modulus at different temperatures.

Temperature (°C)	Yield Strength σ_y (MPa)	Elastic Modulus E (GPa)
RT (≈ 25)	140	86
75	140	86
100	138	71
150	140	66
200	130	65
250	110	62
300	87	32

A plot of the elastic modulus, normalized by the modulus obtained at RT, versus temperature is shown in Figure 7. A clear drop can be noticed in the elastic modulus at temperatures exceeding 100 °C. Further, and a more significant reduction in stiffness was measured at 300 °C. The Eurocode EN1999-1-2 [36] listed stiffness for aluminum alloys at elevated temperatures is also shown in Figure 7. Despite the similarity in the general trend, it is noted that the 5083-H111 alloy considered in the current study exhibited a more pronounced degradation in stiffness, in particular around 300 °C. Accounting for this variation in stiffness is important in external strengthening applications, as the aluminum alloys may be subjected to elevated temperatures in the case of fire exposure.

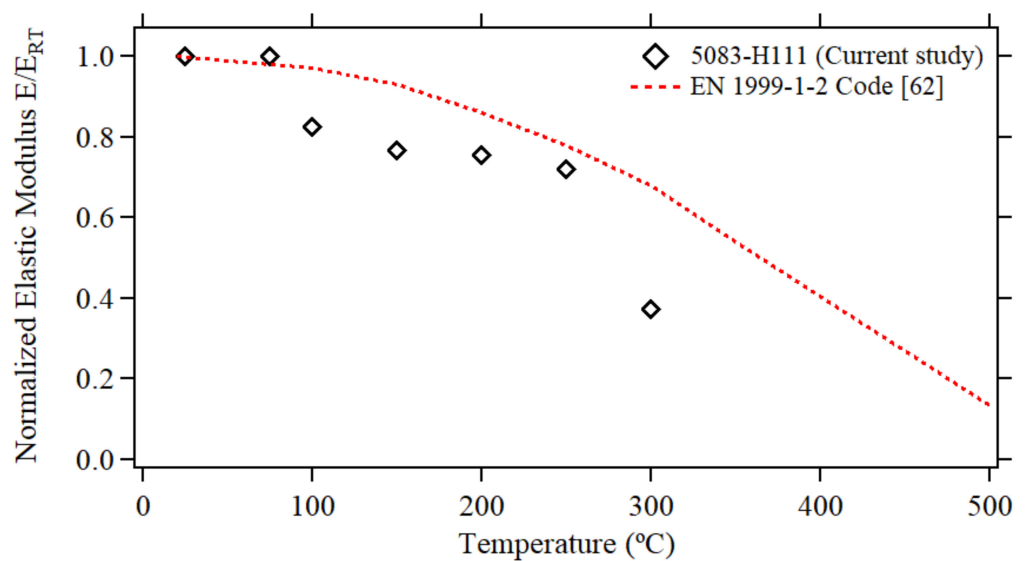


Figure 7. Normalized elastic modulus versus temperature (normalized by the RT elastic modulus).

The yield strength normalized plot is shown in Figure 8. It is clear from Figure 8 that the normalized yield strength was constant up to 150 °C, after which it started to experience degradation in its magnitude with further temperature increase. At 300 °C, the alloy retained about 60% of its original strength which is significantly higher than the $\approx 20\%$ lower limit listed in EN1999-1-2 [36]. The delayed drop in strength is obviously advantageous for the considered structural strengthening applications.

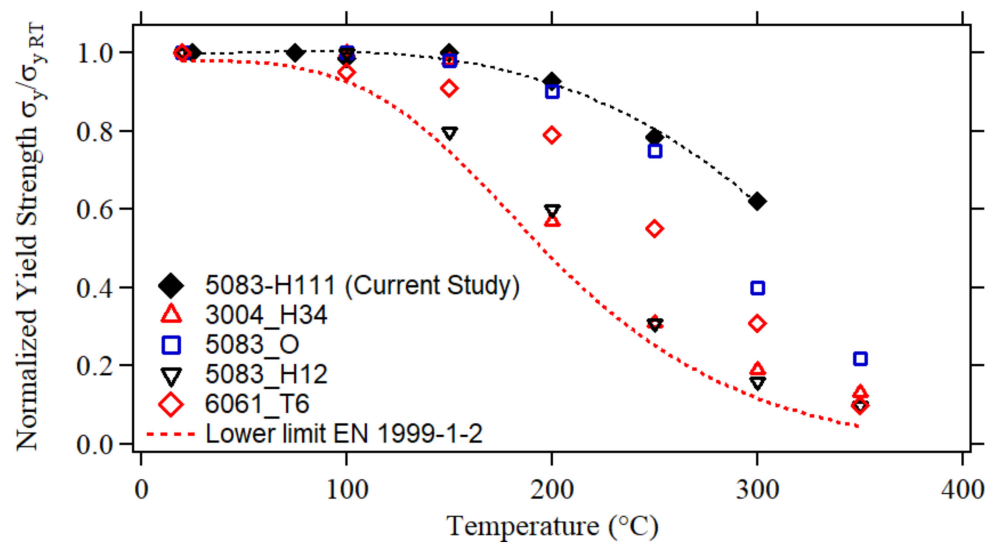


Figure 8. Normalized yield strength versus temperature (normalized by the RT yield strength).

3.2. Predictive Modeling Using the Mechanical Threshold Strength Model

The mechanical threshold strength model (MTS) defines the constitutive material response as a function of strain rate and temperature [30,31]. This physically based model was developed to capture the thermally activated interactions between dislocations and obstacles. Successful calibration of this model for similar 5-xxx series (Al-Mg), which is solid solution strengthened, has been reported in the literature [33]. To the best of the authors’ knowledge, MTS model parameters specifically for AA 5083-H111 have not been established and therefore, it will be conducted in this work.

Based on the MTS model, the strain, temperature, and strain rate dependent flow stress is given using the following Equation (1):

$$\sigma_y(\epsilon_p, \dot{\epsilon}, T) = \sigma_a + (S_i\sigma_i + S_e\sigma_e) \frac{\mu(T)}{\mu_0} \tag{1}$$

The flow stress captures the deformation history (ϵ_p), strain rate ($\dot{\epsilon}$), and temperature impact (T) on the flow stress. The athermal parameter (σ_a) is typically a function of the material microstructure such as grain size and dislocation density. As all samples were made from the same material, thus having an identical structure, σ_a is assumed constant and independent of temperature. The thermal term σ_i describes the yield stress while σ_e is the strain hardening component of the flow stress (captures the evolution of structure beyond initial yielding), μ_0 represents the shear modulus at 0 K. The factors S_i (yielding) and S_e (hardening) are defined using the following Equations (2) and (3):

$$S_i(\dot{\epsilon}, T) = \left[1 - \left(\frac{k T}{g_{0i} b^3 \mu(T)} \ln \frac{\dot{\epsilon}_{0i}}{\dot{\epsilon}} \right)^{\frac{1}{q_i}} \right]^{\frac{1}{p_i}} \tag{2}$$

$$S_e(\dot{\epsilon}, T) = \left[1 - \left(\frac{k T}{g_{0e} b^3 \mu(T)} \ln \frac{\dot{\epsilon}_{0e}}{\dot{\epsilon}} \right)^{\frac{1}{q_e}} \right]^{\frac{1}{p_e}} \tag{3}$$

where b is the burgers vector, k is the Boltzman, $\dot{\epsilon}$ is the deformation strain rate (constant in this work), $\dot{\epsilon}_{0i}$ and $\dot{\epsilon}_{0e}$ are reference strain rates (fitting constants), (q_i, p_i, q_e, p_e) are constants, (g_{0i}, g_{0e}) are the normalized activation energies (for dislocation glide), and $\mu(T)$ is the temperature dependent shear modulus.

As this work emphasis is on establishing the yield strength and not the full constitutive behavior, the thermal component of the flow stress that captures the hardening response can be set to zero (i.e., $\sigma_e = 0$ in Equation (1) as the plastic strain is zero), then initial yielding (yield strength) can be written as follows:

$$\sigma_y(\dot{\epsilon}, T) = \sigma_a + \left(\left[1 - \left(\frac{k T}{g_{0i} b^3 \mu(T)} \ln \frac{\dot{\epsilon}_{0i}}{\dot{\epsilon}} \right)^{\frac{1}{q_i}} \right]^{\frac{1}{p_i}} \right) \frac{\sigma_i \mu(T)}{\mu_0} \tag{4}$$

The parameters listed in Equation (4) can be determined experimentally from the collected stress–strain data, at different temperatures, in this work.

3.3. Determination of the MTS Model Parameters

The thermal parameter σ_a in Equation (4) is constant as all samples were made from the same material and have an identical structure. Therefore, the magnitude of this component is temperature independent and will be less than the lowest yield strength determined experimentally for all the samples ($\sigma_y @ 300^\circ\text{C} = 87 \text{ MPa}$). A value of 80 MPa resulted in a good fit with the experimental data.

The temperature dependent parameter $\mu(T)$ represents the shear modulus of the alloy. For cubic materials, the shear modulus is related to the elastic modulus and Poisson’s ratio using Equation (5):

$$\mu = \frac{E}{2(1 + \nu)} \tag{5}$$

where E is the elastic modulus, and $\nu = 0.33$ is the Poisson’s ratio. Using Equation (5) and the experimentally determined elastic modulus at different temperatures, the shear modulus at each temperature was calculated. The following commonly used empirical relation was used to fit the data as presented by Varshni [37].

$$\mu(T) = \mu_0 - \frac{D_\mu}{\exp\left(\frac{T_{0\mu}}{T}\right) - 1} \tag{6}$$

where μ_0 is the shear modulus at zero K (constant), D_μ and $T_{0\mu}$ are fitting constants. By fitting to the experimental data, the constant in Equation (6) were determined as shown below:

$$\mu(T) = 40811 \text{ MPa} - \frac{3173 \text{ MPa}}{\exp\left(\frac{83}{T}\right) - 1} \tag{7}$$

To find the remaining MTS model parameters in Equation (4), $y = [(\sigma_y - \sigma_a) / \mu(T)]^{p_i}$ was plotted versus $x = \left[\frac{k T}{\mu(T) b^3} \ln \left(\frac{\dot{\epsilon}_{0i}}{0.0003} \right) \right]^{\frac{1}{q_i}}$. With the correct selection of the constants p_i , q_i , and $\dot{\epsilon}_{0i}$, all the data points from different temperatures will unify on a straight line as shown in Figure 9. The reference strain rate, $\dot{\epsilon}_{0i}$, takes values between 1×10^5 and $1 \times 10^{10} \text{ s}^{-1}$. A value of $5 \times 10^8 \text{ s}^{-1}$ has been suggested for A 5183 aluminum alloy [35]. For the material investigated in this work, a value of $5 \times 10^6 \text{ s}^{-1}$ was found to better fit the experimental data. As for p_i (typically 1 or 1/2) and q_i (≥ 1), typical values for A 5183 are in the range of 1/2 and 3/2, respectively. A good fit with the data for AA 5083 was obtained with $p_i = 1$, and $q_i = 3/2$. It should be noted that the data were fitted in the range of 150–300 °C is shown in Figure 9. The yield strength displayed no change at temperatures below 150 °C. The selected values for p_i , q_i , and $\dot{\epsilon}_{0i}$ have clearly unified the data point into a single straight line.

Table 2. MTS model parameters.

MTS Model Parameter (Equation (4))	Value	MTS Model Parameter (Equation (4))	Value
μ	$\mu_0 - \frac{3173 \text{ MPa}}{\exp(\frac{83}{T}) - 1}$	μ_0	40,811 MPa
σ_a	80 MPa	p_i	1
$\dot{\epsilon}_{0i}$	$5 \times 10^6 \text{ s}^{-1}$	q_i	$\frac{3}{2}$
g_{0i}	0.425	$\frac{\sigma_i}{\mu_0}$	0.007
k_b	$1.38064852 \times 10^{-23} \text{ J/K}$	b	$2.86 \times 10^{-10} \text{ m}$

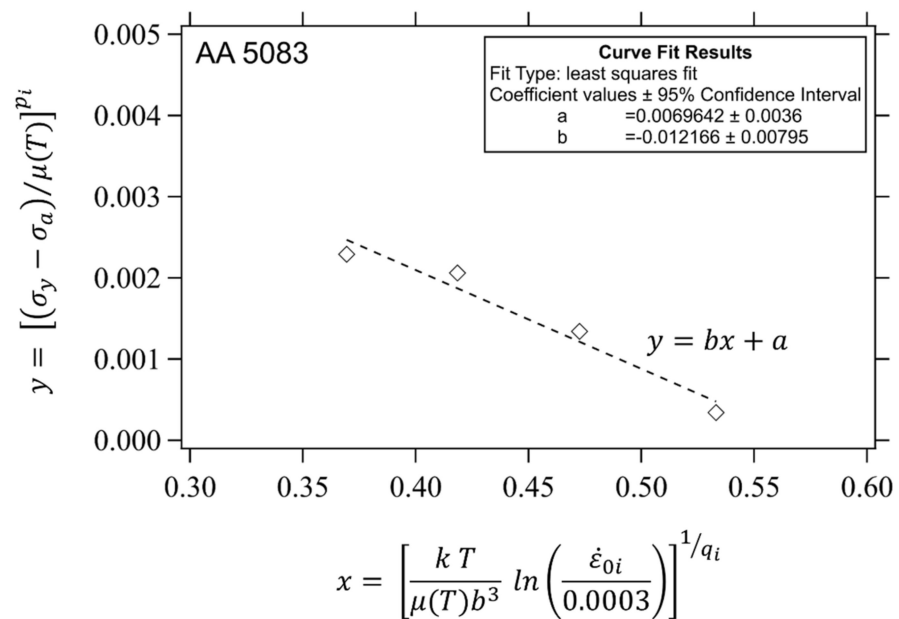


Figure 9. Yield strength and MTS model fit for temperature range 150–300 °C and constant strain rate of $3 \times 10^{-4} \text{ s}^{-1}$. Model parameters are given in Table 2.

By fitting a straight line to the data plotted in Figure 9, the final parameters of the MTS model (i.e., σ_i and g_{0i}) can be determined. For clarity, Equation (4) can be rearranged to the following form:

$$y = \left(\frac{\sigma_y - \sigma_a}{\mu} \right)^{p_i} = \left(\frac{\sigma_i}{\mu_0} \right)^{p_i} - \left(\frac{\sigma_i}{\mu_0} \right)^{p_i} \left(\frac{1}{g_{0i}} \right)^{\frac{1}{q_i}} \left[\frac{k T}{\mu b^3} \ln \left(\frac{\dot{\epsilon}_{0i}}{0.0003} \right) \right]^{\frac{1}{q_i}} \quad (8)$$

from the linear fit in Figure 9, $\left(\frac{\sigma_i}{\mu_0} \right)^{p_i} = \left(\frac{\sigma_i}{\mu_0} \right)^1 = 0.0069$. Additionally, $\left(\frac{\sigma_i}{\mu_0} \right)^{p_i} \left(\frac{1}{g_{0i}} \right)^{\frac{1}{q_i}} = 0.0122$ Consequently, $g_{0i} = 0.425$. A summary of all the model parameters is given in Table 2. The final form of Equation (4) giving the yield strength as a function of temperature is given using:

$$\sigma_y(T) = 80 \text{ MPa} + \left(\left[1 - \left(\frac{k T}{0.425 b^3 \mu(T)} \ln \frac{5 \times 10^6}{0.0003} \right)^{\frac{2}{3}} \right] \right) 0.0069 \mu(T) \quad (9)$$

The final result presented in Equation (9) has been calibrated between 150–300 °C at a constant strain rate of $3 \times 10^{-4} \text{ s}^{-1}$. Between RT ($\approx 25 \text{ }^\circ\text{C}$) and 150 °C, the yield strength is constant. Comparison between experimental data and model prediction results is provided in Section 3.5.

3.4. Elastic Modulus Temperature Dependence

The magnitudes of the experimentally measured elastic moduli revealed degradation in E with temperature increase (as shown in Figure 7) and a pronounced sudden drop at the highest temperature considered in this work (i.e., 300 °C). The empirical relation introduced by Varshni [37] has been typically used to capture the elastic constants temperature dependence of metals due to its simplicity and ability to adequately capture experimental data [38–40]. The model takes the following form:

$$E(T) = E_0 - \frac{D_E}{\exp\left(\frac{T_{0E}}{T}\right) - 1} \tag{10}$$

where T is the temperature in K and, E_0 is the elastic modulus at zero K, D_E and T_{0E} are constant. By fitting to the experimental data, the model parameters can be determined, as presented in Equation (11):

$$E(T) = 109.1 \text{ GPa} - \frac{7.28 \text{ GPa}}{\exp\left(\frac{71.4}{T}\right) - 1} \tag{11}$$

It should be noted that the data point at 300 °C has been omitted from the fit reported in Equation (11) due to the significant drop in the magnitude of the elastic modulus at this temperature. This potentially points to changes in the microstructure such as recrystallization which the model cannot account for. A comparable trend with pronounced reduction in the elastic modulus magnitude has been reported by others on a similar 5083 alloy (AA 5083-H116) at a temperature around 250 °C [41]. The model provided here is therefore valid for temperatures up to 250 °C. A comparison between model prediction and experimental data is provided in the next section.

3.5. Comparison between Experimental Results and Model Predictions

The MTS model predictions for the yield strength (σ_y) as a function of temperature is shown in Figure 10 along with the experimentally determined values. The model prediction is in very good agreement with the experimental results (150–300 °C). At temperatures between 25 and 150 °C, a constant yield is observed and thus the model was not applied to that range. It is noted that similar trends in the yield strength for other aluminum alloys have been reported in the literature. For example, a constant yield up to ≈ 100 °C was shown for AA 5083-H116 followed by a degradation at higher temperatures [41]. Full statistical analysis of the model predictions and the accuracy of the model are provided in Table 3. A small Normalized Mean Square Error (NMSE = 0.04), Mean Absolute Percent Error (MAPE) ranging between 2.40% and 5.27%, and correlation coefficient (R) of 0.98 were calculated. The results demonstrate the ability of the model to capture the obtained experimental data.

Table 3. Performance of model’s prediction compared to experimental results.

Performance Criterion	RMSE (MPa)	NMSE	MAE (MPa)	MAPE (%)	Minimum Absolute Error (MPa)	Maximum Absolute Error (MPa)	Correlation Coefficient (R)
Yield Strength σ_y	3.87	0.04	3.72	3.17	2.40	5.27	0.98
Elastic Modulus E	4.58	0.22	3.84	5.05	0.59	8.88	0.90

RMSE—Root Mean Square Error; NMSE—Normalized Mean Square Error; MAE—Mean Absolute Error; MAPE—Mean Absolute Percent Error; R—Correlation Coefficient.

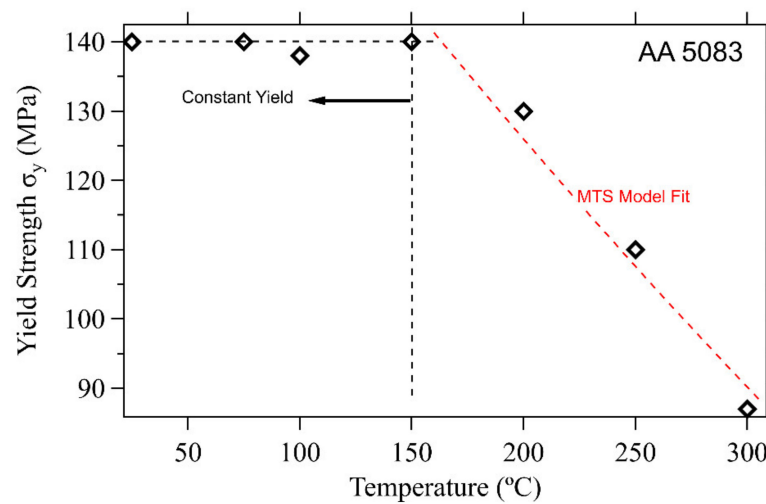


Figure 10. Yield strength MTS model prediction versus temperature (150–300 °C).

The elastic modulus model prediction (Equation (11)) versus temperature is plotted in Figure 11. Good agreement with the experimental data was obtained as shown in Figure 11. Table 3 lists the results of the statistical analysis comparing the model predictions to that of the experimental data. A Normalized Mean Square Error (NMSE = 0.22), Mean Absolute Percent Error (MAPE) ranging between 0.59% and 8.88%, and correlation coefficient (R) of 0.90 were calculated. Thus, the fitted model can reasonably predict the elastic modulus of the AA 5083 plates as a function of increasing temperature.

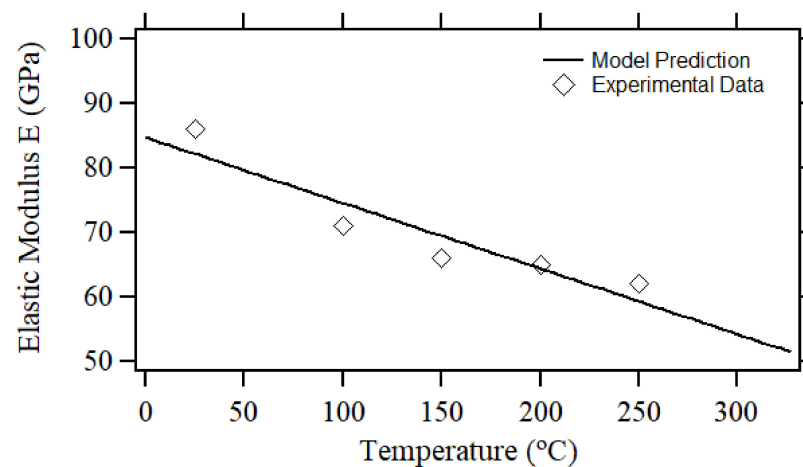


Figure 11. Elastic modulus versus temperature. Experimental data and model prediction.

4. Discussion

In this work, a strong temperature dependence in the yield strength was observed in the temperature range of 150–300 °C, dropping by about 40% at 300 °C. The constant yield strength at temperatures <150 °C has been experimentally observed for various aluminum alloys. For example, 5083-H116, 5083-H321, and 5082 [33,41]. Chen et al. [33] investigated this aspect in a 5182 aluminum alloy, where they discussed three different regimes of deformation at different temperature and strain rate levels. The thermally activated process of dislocation accumulation and recovery becomes significant at higher temperatures and results in temperature dependence in the yield stress. It is in this thermally activated region that the deformation response can be described using the MTS model. The stress–strain curves shown in Figure 5 clearly show a change in deformation mechanism; at RT, strain aging was observed (serrated flow) with positive strain hardening compared to no serrated flow and a reduction in the hardening rate at elevated temperatures. These changes at high

temperatures are indicative of a thermally activated process which would, consequently, explain the lack of temperature dependence in the yield strength initially.

The MTS model has been used effectively to predict the experimentally computed yield strength in the temperature range where thermal effects became significant. Despite the fact that the final outcome (Equation (9)) is rather simple, the model is physically based and capable of capturing the thermally activated process affecting the flow stress at temperatures below 300 °C. At temperatures beyond the explored range in this work (>300 °C), a careful assessment must be conducted to check if the model can be extrapolated to higher temperatures. Based on data available in the literature, it is expected that changes in the deformation mechanisms and creep rates at temperatures beyond 300 °C would hinder the ability to use the MTS model [41,42]. It should be also noted that the models presented in this study are a result of calibration on the provided experimental data. Hence, the consistency and accuracy of the models are dependent on the given geometrical and test conditions. According to Montuori et al. [43], many doubts arise from the accuracy of any proposed constitutive law due to simplifying and eliminating possible sophistications that hinders the fitting of the test results. Therefore, it is important to verify how much this variability is important in terms of determining the mechanical properties of the investigated material. It is finally worth noting that, although outside the scope of this work, the MTS model can also be fitted to capture the hardening response and strain rate sensitivity of the material. Additional experimental data at different strain rates will be needed to accomplish this task.

The experimentally determined elastic modulus experienced a sharp transition between 250 and 300 °C. As discussed above, this is the temperature range where recrystallization and recovery processes are triggered. In addition, the creep behavior has been reported to transition from having initial primary creep (<250 °C) to primarily secondary, steady-state, creep at higher temperatures [44].

The use of AA strengthening plates has been proven to improve the shear and flexural capacity of RC beams. In this work, additional insight, experimentally and through predictive models, into the degradation of mechanical properties of the strengthening material with temperature, is provided. However, the direct impact on strengthening effectiveness has not been explored. A full quantitative assessment dedicated to measure the strengthening effectiveness as a function of stiffness drop and yield strength reduction is worth exploring. It should be pointed out, however, that the use of AA-5083 is not recommended at temperatures exceeding 65 °C for an extended time [45,46]. Despite the many desirable characteristics that include its exceptional performance in extreme and harsh environments (e.g., high resistance to attack by saline seawater and industrial chemicals), the presence of more than 3.5% of magnesium content (Mg) renders this alloy susceptible to stress corrosion cracking, and accordingly limits the operational temperature range. Since the use of AA-5083 as a strengthening material for RC beams is unlikely to involve exposure to high temperature for an extended period, such limitation may have little, if any, effect on performance.

5. Conclusions

This paper experimentally investigated the degradation in the mechanical properties of aluminum alloy AA 5083 plates when exposed to temperatures ranging from 25 to 300 °C. Analytical models for the elastic modulus and for the yield strength of AA 5083 plates, as a function of temperature, were developed based on the obtained experimental results. Both analytical models showed reasonable accuracy in predicting the elastic modulus and the yield strength at the specified temperature range from 25 to 300 °C.

The work supports the following conclusions:

1. The AA 5083 aluminum sheets displayed degradation in the elastic modulus with temperature increase. Up to 250 °C, the total reduction in the modulus was less than 25% compared to the RT value. A huge drop was observed beyond this temperature range, reaching ≈60% reduction at 300 °C. An empirical model fit to the experi-

mental data (up to 250 °C) resulted in good predictive capability in the temperature range considered.

2. At low to moderate temperatures, the yield strength was constantly experiencing no change up to 150 °C. With further temperature increase, reduction in the yield strength is triggered, resulting in a total reduction of 40% at 300 °C. The yield strength in the region/temperature range experiencing degradation was captured using the MTS model with good accuracy.
3. Based on the fact that significant reduction in the elastic modulus occurs above 250 °C, it is not recommended to use this alloy in that temperature range. From a strength perspective, temperatures below 150 °C assure no reduction in the load capacity before plastic deformation commences. In practical strengthening applications under normal conditions, 150 °C provides a good margin of safety against loss of strength and plastic deformation. However, it is conceivable to reach higher temperatures in abnormal circumstances such as fire exposure. To provide additional margin before strengthening failure, it is recommended to provide insulation to the externally bonded AA plates to prevent a significant spike in temperature under such conditions.

Author Contributions: Conceptualization W.A., R.H. and J.A.; methodology, W.A. and R.H.; software, W.A.; validation, W.A., R.H. and J.A.; formal analysis, W.A.; investigation, W.A. and R.H.; resources, J.A.; data curation, W.A.; writing—original draft preparation, W.A.; writing—review and editing, R.H. and J.A.; visualization, W.A. All authors have read and agreed to the published version of the manuscript.

Funding: This research received no external funding.

Data Availability Statement: Data is contained within the article.

Acknowledgments: This research project was supported by the American University of Sharjah (AUS). Their support is highly acknowledged.

Conflicts of Interest: The authors declare no conflict of interest.

References

1. Chen, F.; Jin, Z.; Wang, E.; Wang, L.; Jiang, Y.; Guo, P.; Gao, X.; He, X. Relationship model between surface strain of concrete and expansion force of reinforcement rust. *Sci. Rep.* **2021**, *11*, 4208. [[CrossRef](#)]
2. de Azevedo, A.R.G.; Marvila, M.T.; Antunes, M.L.P.; Rangel, E.C.; Fediuk, R. Technological Perspective for Use the Natural Pineapple Fiber in Mortar to Repair Structures. *Waste Biomass Valor.* **2021**. [[CrossRef](#)]
3. Maljaars, J.; Twilt, L.; Fellingner, J.H.H.; Snijder, H.H.; Soetens, F. Aluminium structures exposed to fire conditions—an overview. *Heron* **2010**, *55*, 85–122.
4. Abdalla, J.A.; Hraib, F.H.; Hawileh, R.A.; Mirghani, A.M. Experimental investigation of bond-slip behavior of aluminum plates adhesively bonded to concrete. *J. Adhes. Sci. Technol.* **2017**, *31*, 82–99. [[CrossRef](#)]
5. Abuodeh, O.R.; Abdalla, J.A.; Hawileh, R.A. Flexural strengthening of RC beams using aluminum alloy plates with mechanically-fastened anchorage systems: An experimental investigation. *Eng. Struct.* **2021**, *234*, 111969. [[CrossRef](#)]
6. Abdalla, J.A.; Mirghani, A.; Hawileh, R.A. Bond stress and behavior of interface between untreated aluminum alloy surface and concrete. *Procedia Struct. Integr.* **2020**, *28*, 1295–1302. [[CrossRef](#)]
7. Abdalla, J.A.; Abu-Obeidah, A.S.; Hawileh, R.A.; Rasheed, H.A. Shear strengthening of reinforced concrete beams using externally-bonded aluminum alloy plates: An experimental study. *Constr. Build. Mater.* **2016**, *128*, 24–37. [[CrossRef](#)]
8. Abdalla, J.A.; Abou-Obeidah, A.S.; Hawileh, R.A. Behavior of Shear Deficient Reinforced Concrete Beams with Externally Bonded Aluminum Alloy Plates. In Proceedings of the 2011 World Congress on Advances in Structural Engineering and Mechanics, Seoul, Korea, 18–23 September 2011.
9. Naser, M.; Hawileh, R.A.; Abdalla, J.A. Use of Fiber-Reinforced Polymer Composites in Strengthening Reinforced Concrete Structures: A Critical Review. *Eng. Struct.* **2019**, *198*, 109542. [[CrossRef](#)]
10. Choobbor, S.S.; Hawileh, R.A.; Abu-Obeidah, A.; Abdalla, J.A. Performance of hybrid carbon and basalt FRP sheets in strengthening concrete beams in flexure. *Compos. Struct.* **2019**, *227*, 111337. [[CrossRef](#)]
11. Al-Thairy, H.; Al-Jasmi, S.K. Numerical Investigation on the Behavior of Reinforced Lightweight Concrete Beams at Elevated Temperature. *Iran J. Sci. Technol. Trans. Civ. Eng.* **2021**. [[CrossRef](#)]
12. Abu-Obeidah, A.; Hawileh, R.A.; Abdalla, J.A. Finite element analysis of strengthened RC beams in shear with aluminum plates. *Comput. Struct.* **2015**, *147*, 36–46. [[CrossRef](#)]

13. Fayed, S.; Basha, A.; Hamoda, A. Shear strengthening of RC beams using aluminum plates: An experimental work. *Constr. Build. Mater.* **2019**, *221*, 122–138. [[CrossRef](#)]
14. Abdalla, J.A.; Abu-Obeidah, A.S.; Hawileh, R.A. Use of Aluminum Alloy Plates as Externally Bonded Shear Reinforcement for R/C Beams. *Procedia Struct. Integr.* **2019**, *17*, 403–410. [[CrossRef](#)]
15. Abu-Obeidah, A.S.; Abdalla, J.A.; Hawileh, R.A. Shear strengthening of deficient concrete beams with marine grade aluminum alloy plates. *Adv. Concr. Constr.* **2019**, *7*, 249–262. [[CrossRef](#)]
16. Rasheed, H.A.; Abdalla, J.A.; Hawileh, R.A.; Al-Tamimi, A.K. Flexural Behavior of Reinforced Concrete Beams Strengthened with Externally Bonded Aluminum Alloy Plates. *Eng. Struct.* **2017**, *147*, 473–485. [[CrossRef](#)]
17. Abuodeh, O.; Abdalla, J.A.; Hawileh, R.A. The flexural behavior of bolting and bonding Aluminum Alloy plates to RC beams. *Procedia Struct. Integr.* **2019**, *17*, 395–402. [[CrossRef](#)]
18. Nimna, S.; Abraham, M. Reinforced Concrete Beam Strengthened with Externally Bonded Aluminum Alloy Plates and CFRP Sheets. *Int. J. Appl. Eng. Res.* **2019**, *14*, 121–125.
19. Xing, G.; Chang, Z.; Ozbulut, O.E. Behavior and failure modes of reinforced concrete beams strengthened with NSM GFRP or aluminum alloy bars. *Struct. Concr.* **2018**, *19*, 1023–1035. [[CrossRef](#)]
20. Xing, G.; Chang, Z.; Ozbulut, O.E. Feasibility of using aluminum alloy bars as near-surface mounted reinforcement for flexural strengthening of reinforced concrete beams. *Struct. Concr.* **2020**, *21*, 1557–1576. [[CrossRef](#)]
21. Yu, X.; Xing, G.; Chang, Z. Flexural behavior of reinforced concrete beams strengthened with near-surface mounted 7075 aluminum alloy bars. *J. Build. Eng.* **2020**, *31*, 101393. [[CrossRef](#)]
22. Summers, P.T.; Matulich, R.D.; Case, S.W.; Lattimer, B. Post-fire mechanical properties and hardness of 5083 and 6082 aluminum alloys. In *ASME International Mechanical Engineering Congress and Exposition*; ASME (American Society of Mechanical Engineers): Houston, TX, USA, 2012; Volume 45196, pp. 1251–1259. [[CrossRef](#)]
23. Summers, P.T.; Case, S.W.; Lattimer, B.Y. Residual mechanical properties of aluminum alloys AA5083-H116 and AA6061-T651 after fire. *Eng. Struct.* **2014**, *76*, 49–61. [[CrossRef](#)]
24. Chen, S.R.; Wu, C.Y.; Ou, Y.L.; Yeh, Y.L. Hot Deformation Resistance of an AA5083 Alloy under High Strain Rate. *Key Eng. Mater.* **2014**, *626*, 553–560. [[CrossRef](#)]
25. Summers, P.T.; Mouritz, A.P.; Case, S.W.; Lattimer, B.Y. Microstructure-based Modeling of Residual Yield Strength and Strain Hardening after Fire Exposure of Aluminum Alloy 5083-H116. *Mater. Sci. Eng. A* **2015**, *632*, 14–28. [[CrossRef](#)]
26. Free, J.C.; Summers, P.T.; Lattimer, B.Y.; Case, S.W. Mechanical Properties of 5000 Series Aluminum Alloys Following Fire Exposure. In *TMS 2016 145th Annual Meeting & Exhibition*; The Minerals, Metals & Materials Society, Ed.; Springer: Cham, Switzerland; Nashville, TN, USA, 2016. [[CrossRef](#)]
27. Guo, X.; Tao, L.; Zhu, S.; Zong, S. Experimental Investigation of Mechanical Properties of Aluminum Alloy at High and Low Temperatures. *J. Mater. Civ. Eng.* **2020**, *32*, 06019016. [[CrossRef](#)]
28. Huda, Z.; Zaharinie, T.; Min, G.J. Temperature effects on material behavior of aerospace aluminum alloys for subsonic and supersonic aircrafts. *J. Aerosp. Eng.* **2010**, *23*, 124–128. [[CrossRef](#)]
29. Prakash, G.; Singh, N.K.; Sharma, P.; Gupta, N.K. Tensile, Compressive, and Flexural Behaviors of Al5052-H32 in a Wide Range of Strain Rates and Temperatures. *J. Mater. Civ. Eng.* **2020**, *32*, 04020090. [[CrossRef](#)]
30. Follansbee, P.S.; Kocks, U.F. A constitutive description of the deformation of copper based on the use of the mechanical threshold stress as an internal state variable. *Acta. Metall.* **1988**, *36*, 81–93. [[CrossRef](#)]
31. Kocks, U.F. Realistic constitutive relations for metal plasticity. *Mater. Sci. Eng. A* **2001**, *317*, 181–187. [[CrossRef](#)]
32. Banerjee, B. The Mechanical Threshold Stress model for various tempers of AISI 4340 steel. *Int. J. Solids Struct.* **2007**, *44*, 834–859. [[CrossRef](#)]
33. Chen, S.R.; Kocks, U.; MacEwen, S.; Beaudoin, A.J.; Stout, M.G. Constitutive Modeling of a 5182 Aluminum as a Function of Strain Rate and Temperature. In Proceedings of the Hot Deformation of Aluminum Alloys II—The Minerals, Metals & Materials Society, Rosemont, IL, USA, 31 December 1998. [[CrossRef](#)]
34. Banerjee, B.; Bhawalkar, A. An extended mechanical threshold stress plasticity model: Modeling 6061-T6 aluminum alloy. *J. Mech. Mater. Struct.* **2008**, *3*, 391–424. [[CrossRef](#)]
35. Ma, R.; Truster, T.J.; Puplampu, S.B.; Penumadu, D. Investigating mechanical degradation due to fire exposure of aluminum alloy 5083 using crystal plasticity finite element method. *Int. J. Solids Struct.* **2018**, *134*, 151–160. [[CrossRef](#)]
36. CEN. *Design of aluminium structures—Part 1-2: Structural fire design (EN 1999-1-2)*; Eurocode 9; CEN: Brussels, Belgium, 2007.
37. Varshni, Y.P. Temperature Dependence of the Elastic Constants. *Phys. Rev. B* **1970**, *2*, 3952–3958. [[CrossRef](#)]
38. Klosowski, P.; Mleczyk, A. Identification of Bodner-Partom Viscoplastic Model Parameters for Some Aluminum Alloys at Elevated Temperature. *J. Mater. Civ. Eng.* **2017**, *29*, 04017034. [[CrossRef](#)]
39. Kandare, E.; Feih, S.; Lattimer, B.Y.; Mouritz, A.P. Larson–Miller failure modeling of aluminum in fire. *Metall. Mater. Trans.* **2010**, *41*, 3091–3099. [[CrossRef](#)]
40. Huskins, E.L.; Cao, B.; Ramesh, K.T. Strengthening mechanisms in an Al–Mg alloy. *Mater. Sci. Eng. A* **2010**, *527*, 1292–1298. [[CrossRef](#)]
41. Summers, P.T.; Chen, Y.; Rippe, C.M.; Allen, B.; Mouritz, A.P.; Case, S.W.; Lattimer, B.Y. Overview of aluminum alloy mechanical properties during and after fires. *Fire Sci. Rev.* **2015**, *4*, 1–36. [[CrossRef](#)]

42. Darras, B.M.; Abed, F.H.; Abdul-Latif, A.; Pervaiz, S. Experimental Investigation of Deformation in 5083 Marine-Grade Aluminum Alloy at Elevated Temperatures. *J. Mater. Eng. Perform.* **2015**, *24*, 1663–1668. [[CrossRef](#)]
43. Montuori, R.; Piluso, V.; Tisi, A. Comparative analysis and critical issues of the main constitutive laws for concrete elements confined with FRP. *Compos. B. Eng.* **2012**, *43*, 3219–3230. [[CrossRef](#)]
44. Allen, B.W. Creep and Elevated Temperature Mechanical Properties of 5083 and 6061 Aluminum. Master of Science, Engineering Mechanics, Virginia Polytechnic Institute and State University. 2012. Available online: <http://hdl.handle.net/10919/52630> (accessed on 20 December 2012).
45. Aluminium Alloy-Commercial Alloy-5083-‘0’-H111 Sheet and Plate. Available online: http://www.aalco.co.uk/datasheets/Aluminium-Alloy-5083-0-H111-Sheet-and-Plate_149.ashx (accessed on 5 June 2021).
46. Atlas Steels Aluminium Alloy Datasheets. Available online: http://www.atlassteels.com.au/documents/Atlas_Aluminium_datasheet_5083_rev_Oct_2013.pdf (accessed on 5 June 2021).